

Utilization of CTR to Measure the Evolution of Electron-Beam

Microbunching in a SASE FEL

A.H. Lumpkin, B.X. Yang, W.J. Berg, Y.C. Chae, J.W. Lewellen,

N.S. Sereno, R.J. Dejus, C. Benson and E. Moog

Advanced Photon Source

Argonne National Laboratory

Argonne, Illinois 60439

Abstract

We report the first measurements of the z-dependent evolution of electron-beam microbunching as revealed through coherent transition radiation (CTR) measurements in a visible self-amplified spontaneous emission (SASE) free-electron laser (FEL) experiment. The increase in microbunching was detected by tracking the growth of the visible CTR signals as generated from insertable metal mirrors/foils after each of the last three undulators. The same optical imaging diagnostics that were used to track the z-dependent intensity of the undulator radiation (UR) were also used to track the electron beam/CTR information. Angular distribution, beam size, and intensity data were obtained after each of the last three undulators in the five-undulator series, and spectral information was obtained after the last undulator. The exponential growth rate of the CTR was found to be very similar to that of the UR and consistent with simulations using the code GENESIS.

1. Introduction

The interest in self-amplified spontaneous emission (SASE) free-electron laser (FEL) physics has been growing in recent years. This has been spurred by some early successes in the cm-wave and far-infrared (FIR) regime [1,2] and the speculation that the process should scale to the x-ray regime [3,4]. Fundamental to the process is the longitudinal microbunching of the electron beam as it copropagates with the undulator radiation (UR) along the length z of the undulators [5-8]. As the fraction of microbunched beam increases along z , so does the coherent radiation that leads to the exponential gain regime. The UR has been routinely measured in several experiments [2,9], but the complementary information in the electron beam has only been measured at the exit of the last (only) undulator in the UCLA/LANL SASE experiment at $13\ \mu\text{m}$ via coherent transition radiation (CTR) [10]. Additionally, a more direct time-domain experiment at Stanford University was able to display the longitudinal striations in the charge distribution at $\lambda=60\ \mu\text{m}$, the wavelength of their oscillator experiment [11]. These experiments were reported in the last two international FEL conferences. The first experiment used the properties of coherent transition radiation generated by the SASE-induced microbunching to test their models [10].

We have taken advantage of an operating SASE FEL in the visible wavelength regime (near $530\ \text{nm}$) to extend the CTR-based techniques to z -dependent angular distribution, beam size, and intensity measurements. The z -dependent growth in intensity is particularly of interest since we find the effective gain length for the UR and CTR so similar, as expected from the microbunching model. In addition, we have obtained hundreds of CTR angular distribution images that exhibit

structures that strongly suggest interference effects in a two-surface geometry, electron-beam/photon-beam overlap effects, and electron-beam pointing information.

These experiments were the culmination of our goals to generate sub-0.5-ps electron beam bunches in a thermionic rf gun resulting in 100-A peak current, to measure such short pulses with a CTR interferometer (and even do this nondestructively with coherent diffraction radiation (CDR)) to characterize the core beam brightness, to demonstrate SASE gain with such a beam, and then to make the microbunching measurements using CTR. The first three goals are addressed in more detail in two complementary papers in these proceedings [12,13]. This paper will focus on the z-dependent microbunching measurements. An estimate of CTR photon intensity has been given by the authors of reference 10 (with additional background in references 14,15). Integration of their equations over angular space results in the following equation:

$$N_{\text{CTR}} \approx \frac{\alpha(N_b b_n)^2}{4\sqrt{\pi}k_r \sigma_z} \left(\frac{\gamma}{nk_r} \right)^4 \left(\frac{\sigma_x^2 + \sigma_y^2}{\sigma_x^3 \sigma_y^3} \right), \quad (1)$$

where α is the fine structure constant, N_b is the number of electrons, b_n is the bunching fraction, k_r is the radiation wave number (and thus the beam modulation wave number), n is the harmonic number, $\sigma_{x,y}$ are the transverse beam sizes, and σ_z is the longitudinal size. It is noted that higher charge intensities and smaller transverse size would enhance CTR production. It is also noted that since our visible wavelength is 20 times shorter than the 13- μm experiment, the number of electrons in a cubic wavelength volume is relatively reduced. However, the fact that the radiation is enhanced at the visible fundamental wavelength (and harmonics) opens up the experiment to imaging diagnostics.

2. Experimental Background

These experiments were performed at the Advanced Photon Source (APS) during operations with a thermionic rf gun beam accelerated to 217 MeV by the S-band linac normally used as part of the injector system for the 7-GeV storage ring [16,17]. This accelerator and diagnostics have been described previously [18]. This beam is transported to the set of five undulators in the Low-Energy Undulator Test Line (LEUTL) tunnel. A schematic of the experiment is given in Fig.1. It is not to scale, and there is an approximately 40-m transport line between the three-screen emittance station and the entrance of the undulators.

In this case the rf gun cavity was operated with a higher gradient than that used for the injection operations, and it was optimized for peak current by use of a CTR interferometer located after the first accelerator at ~ 40 MeV energy [12]. This optimization process was critical to the eventual success of the experiments. The rf gun includes an α magnet to inject the beam into the linac (see Fig. 1). We determined that there is a sensitive balance of rf gun gradient, gun current, α -magnet current, α -magnet scraper setting (low energy), and rf phasing to be investigated. A scan of the α -magnet current was done first to find the peak CTR signal. The CTR signal depends directly on N_b^2 and inversely on the bunch length. The position of the low-energy scraper in the α -magnet chamber was also scanned, and the beam relative intensity from a rf beam position monitor (BPM) sum signal and the CTR signal recorded. A clear N_b^2 dependence of the CTR for the core of the beam was observed. The scraper also rejects the low energy tail of the beam distribution with its inferior emittance. The interferometer scans were performed with several

scraper settings to verify the core had been selected in the longitudinal profile. A bunch length of ~ 450 fs (FWHM) was calculated as described in reference [12]. An example of the longitudinal profile is shown in Fig. 2. The 450-fs (FWHM) distribution is almost an order of magnitude shorter than the APS photocathode (PC) gun's micropulse also used in SASE experiments this year [9], but it also has correspondingly less charge. Since the slippage length ($N\lambda$) is about $180 \mu\text{m}$ in the visible experiment, the rf gun micropulse length is comparable to it. The charge was measured in a downstream Faraday cup, and the peak current determined to be about 100 A.

The beam was then transported to the LEUTL tunnel [19], where a set of five undulators with a total magnetic structure length of 12.0 m is installed. The properties of the undulators and the diagnostics stations have been previously described [20]. Very briefly, the undulator cells have a period of 3.3 cm and a length $L=2.4$ m. They have a fixed gap with a field parameter $K=3.1$. There is a roughly 0.38-m space between each undulator. This space is used for diagnostics and focusing and steering elements before the first undulator and after each of the five installed undulator sections. A schematic of these stations is shown in Fig. 3. The screens on the first actuator include positions for a YAG/mirror, a mirror at 45° , and a thin ($6\text{-}\mu\text{m}$) Al foil mounted with its surface normal to the beam direction (in the last three stations). This thin foil serves two functions: 1) to block the strong, visible UR, and 2) to generate optical transition radiation (OTR) or CTR as the e-beam transits the foil/vacuum interfaces. A digital camera views the e-beam images from the YAG and the reflected undulator radiation from the mirror. The second actuator, located 63 mm downstream, involves a retractable mirror at 45° to the beam direction and another digital camera and lens for both near-field and far-field (focus at infinity) imaging. This visible light detector

(VLD) system provides both beam size and angular distribution data, respectively. Both neutral density (ND) filters and bandpass (BP) filters are selectable by two filter wheels in front of the cameras.

Since the UR is more than 500 times brighter than OTR/CTR after undulator 5, the thin opaque foil was critical to separating the two sources of radiation. Bandpass filters could not be used to see the enhanced CTR with UR present because it is predicted to be at or near the fundamental wavelengths of the SASE [10]. The camera system that views the 45° mirror can thus be used to obtain the UR and the off-axis radiation out to ± 10 mrad as well as the OTR/CTR radiation. For OTR the opening angle is expected at $\pm 1/\gamma = 2.3$ mrad where γ is the Lorentz factor. The estimate of the diffraction-limited CTR cone angle [10] for an axisymmetric beam of size σ (100 μm) is $\theta_d = (\sqrt{2} nk_r \sigma)^{-1} = 0.6$ mrad. Since the spacing between the foil and the second metal mirror is similar to the formation length $\gamma^2 \lambda \approx 90$ mm, we actually see interference phenomena in the CTR signals in analogy to OTR interferometers [21,22].

At the end of the last undulator a remotely controlled pickoff mirror can be used to redirect the UR or CTR to an Oriel UV-visible spectrometer. Spectral effects were also observed in the angular distribution data using bandpass filters. The basic experiments involved the acquisition of digital images of the UR after each of the undulators. After verifying there was noticeable z-dependent intensity growth in the UR, the CTR data were recorded by inserting the thin Al foil at each station. Both near-field and far-field data were taken so e-beam source size and the angular distribution data were available.

3. Microbunching Results and Discussion

3.1 Experimental Results (z-dependent)

The evolution of the electron beam's microbunching is revealed in the evolution of the angular distribution images at stations VLD 0, 3, 4, 5. The VLD 0 station is unique in that it has no undulator before it and no installed thin, blocking foil in the Y0 location. In Fig. 4a the dim angular distribution image of the OTR from the single 45° mirror at VLD 0 is shown. The opening cone angle is consistent with the expected $1/\gamma=2.3$ mrad for the 217-MeV beam. However, at the end of undulator 3, we see striking changes in the Fig. 4b VLD 3 image (also with focus at infinity). The inner lobes are at about ± 1.9 mrad, and there are two vertically-localized hot spots on the inner lobes. There are weak indications of other vertical fringes at -4.4 mrad. In Fig. 4c the VLD 5 image indicates an asymmetric evolution since only the lower vertical peak is enhanced by about a factor 40 over the VLD 3 peak. Note the neutral density filter (ND) change from 0.0 to 1.0 and the vertical intensity scale change from 100 to 200 between the VLD 3 (4b) and VLD 5 (4c) data, respectively.

Initial assessments of these and other images support the interpretation that the fringes are indeed due to the interference of the two CTR sources, the forward CTR from the thin foil and the backward CTR from the 45° pickoff mirror. The vertical angle fringe locations can be reproduced within about 10% by our existing OTR interferometer code. The breaking of the azimuthal symmetry of the CTR images is related to the nonaxisymmetric e-beam transverse size (2-3 times larger horizontally) as clarified mathematically with the bunch form factors [23] and to the misalignment of the beams. In Fig. 5 the calculated interference pattern is shown for a beam divergence of 0.4 mrad, wavelength interval of 500-580 nm, and foil spacing of 63 mm.

Since no known polarized optical component is in front of the camera, the angular distribution would involve the contribution from both parallel (ipar) and perpendicular (iperp) polarization components or the total (w) signal indicated by the thin, solid-line curve. For completeness the curve denoted tau is the difference over the sum of the two polarization components. Full symmetry would be expected in the OTR and anticipated in the CTR if the longitudinal microbunching occurs uniformly in the transverse slice. This is evidently not the case.

Processing of the hundred images taken at each z location was performed and the averaged intensity growth tracked. In Fig. 6 we see the clear exponential signature corresponding to a gain length $L_g=1.3$ m in the UR (SASE) signals represented by the diamond symbol. The ~500 times weaker CTR signal (plus symbol) has a very similar gain length fitted at 1.4 m. The CTR angle-integrated (and wavelength integrated) data (square symbol) show the longer gain length of 2.3 m. We attribute the bright peaks in the CTR images to the microbunching on the fundamental at 537 nm.

3.2 GENESIS Code Results

We also used the code GENESIS [24] to calculate the z-dependence of the bunching fraction with the electron beam parameters ($\epsilon_{nx}=16$ π mm mrad, $\epsilon_{ny}=8$ π mm mrad, $I_{peak}=100$ A, and $\sigma_E=0.1\%$) and an assumed match into the undulators. Figure 7 shows a plot of the exponential growth of the UR. The approximate gain length is consistent with the data of Fig. 6. In Fig. 8 the calculated bunching fraction of 0.2% at the end of undulator 5 with a factor of 8 increase after

undulator 1 is also consistent with the CTR growth using Eq. (1). Additionally, the observed e-beam transverse size of $\sigma_x=200 \mu\text{m}$, $\sigma_y=120 \mu\text{m}$ using the CTR data after undulator 5 is smaller horizontally than expected, and this may relate to the enhanced emissions of the transverse core of the beam. An average gain length of $\sim 1.6 \text{ m}$ is calculated over all five undulators, which is in reasonable agreement with the experiment and the value of 1.3-1.6 m based on Xie's parameterization of SASE gain [25]. The sub-0.5-ps electron bunch also leads to a GENESIS-calculated narrow optical pulse that may have relevance to eventual user experiments.

3.3 UV-Visible Spectrometer Data

On a separate run with PC-gun beam in July, 2000 we have obtained the evidence of spectral narrowing. OTR has a broad-band spectrum through the visible regime, but under the SASE gain conditions we see distinct narrow-band, CTR emissions at the fundamental consistent with Eq. (1) when the thin foil is inserted after undulator 5. Figure 9 shows an example of the UR spectrum and the CTR spectrum. The ND filters at the entrance of the spectrometer were used to attenuate, by at least 100, the brighter UR signal. There is an indication that the CTR spectral width is a little larger than that of UR. Due to the shot-to-shot energy jitter there is no definitive evidence of a small centroid shift as reported by the authors of reference 10.

4. Summary

In summary, we have evidence for the direct verification of the bunching fraction evolution using CTR along the undulators in a visible light SASE FEL experiment. The intensity growth rate in the CTR signal is similar to the UR growth rate as predicted. In addition, the angle-resolved data images reveal for the first time interference effects as well as localized, hot spots

(peaks) in the distribution. These features may be used to optimize the critical coalignment of the electron beam and photon beam and thus to optimize FEL performance. We look forward to further experiments at higher gain with nine undulators and development of a more complete model of these effects.

5. Acknowledgements

The authors acknowledge discussions with J. Rosenzweig (UCLA) and A. Tremaine (UCLA) on FIR CTR issues; the assistance of M. Erdmann and T. Powers; the comments of J. Lewellen and S. Milton; and the support of G. Decker, P. Den Hartog, K.J. Kim, and J. Galayda (all of APS).

This work is supported by the U.S. Department of Energy, Office of Basic Energy Sciences, under contract No. W-31-109-ENG-38.

References

1. T. J. Orzechowski et al., NIM A250, 144 (1986).
2. M. Hogan et al., Phys. Rev. Lett. 81, 4897 (1998).
3. K.-J. Kim, NIM A393, 147 (1997).
4. J. Rossbach, "Recent SASE Free Electron Laser Results," Proceedings of EPAC 2000, Vienna, June 25-30, 2000, and references therein, to be published.
5. Y. S. Derbenev, A. M. Kondratenko, and E. L. Saldin, NIM A193, 452 (1982).
6. R. Bonifacio, C. Pellegrini, and L. Narducci, Opt. Comm. 50, 373 (1984).
7. K.-J. Kim, NIM A250, 396 (1986).
8. J.-M. Wang and L. H. Yu, NIM A250, 484 (1986).
9. S. V. Milton et al., "Observation of SASE and Exponential Growth at 530nm," Phys. Rev. Lett. 85, 988 (2000).
10. A. Tremaine et al., Phys. Rev. Lett. 81, 5816 (1998).
11. Kenneth N. Ricci and Todd I. Smith, Phys. Rev. Special Topics - Accelerators and Beams, Vol. 3, 032801-1 (2000).
12. A.H. Lumpkin et al., "Development of a Coherent Transition Radiation-Based Bunch Length Monitor with Application to the APS rf Thermionic Gun Beam Optimization," these proceedings.
13. A.H. Lumpkin et al., "First Measurements of sub-picosecond Electron-Beam Structure by Autocorrelation of Coherent Diffraction Radiation," these proceedings.
14. Yukio Shibata et al., Phys. Rev. E50, 1479 (1994).
15. J. B. Rosenzweig, G. Travish, and A. Tremaine, NIM A365, 255 (1995).

16. J. W. Lewellen et al., Proc. of the 1998 Linac Conference, Chicago, ANL-98/28, Vol. 2, 863 (1999).
17. M. Borland, Proc. of the 1993 Particle Accel. Conf., New York, 3015 (1993).
18. A.H. Lumpkin, W.J. Berg, B.X. Yang, and M. White, "Time-Resolved Imaging for the APS Linac Beams," Proc. of the 1998 Linac Conference, Chicago, ANL-98/28 Vol. 1, 529 (1999).
19. S. V. Milton et al., NIM A407, 210 (1998).
20. E. Gluskin et al., NIM A429, 358 (1999).
21. L. Wartski et al., J. Appl. Phys. 46, 3644 (1975).
22. A. H. Lumpkin et al., NIM A296, 150 (1990); D.W. Rule et al., Idem, p. 7389.
23. Z. Huang, Argonne National Laboratory, private communication, September 2000.
24. S. Reiche, "GENESIS 1.3: A fully 3D time-dependent FEL Simulation Code," NIM A429, 243 (1999).
25. M. Xie, Proc. of the 1995 Particle Accel. Conf., Dallas, Texas, 183 (1995).

Figure Captions

- Fig. 1 A schematic of the APS SASE FEL experiment. The electron beam gun sources, the linac, the CTR/CDR interferometer station, the electron beam spectrometers, and the undulators with some diagnostics are indicated.
- Fig. 2 An example of the electron-beam longitudinal profile as calculated from the CTR autocorrelation. A bunch length of ~ 450 fs (FWHM) is indicated.
- Fig. 3 A detailed schematic of the diagnostics and beam matching station before and after each undulator. The first actuator includes positions for a YAG:Ce crystal plus 45° mirror, a 45° mirror, and a thin Al foil (after the last three undulators). The second actuator holds a mirror whose surface is at 45° to the beam direction. A digital camera with ND filters and BP filters is used to view each inserted screen.
- Fig. 4 A composite of OTR and CTR angular distribution images obtained at the VLD 0, 3, and 5 positions. Note ND filter values and the changes in image intensity along the z direction of the undulators. The θ_x and θ_y distributions are indicated with a y-intensity profile (sampled through the center of the pattern) displayed on the right hand side..
- Fig. 5 A calculated OTR interferogram that reproduces the fringe pattern observed in the angular distribution images.
- Fig. 6 The z dependence of SASE signal, CTR peak signal, and angle-integrated CTR signal with the thermionic rf gun beam. The SASE UR is about 200 times brighter than the CTR, but growth rates are very similar as expected from microbunching models.
- Fig. 7 GENESIS code results for the growth of UR along the undulators using the measured properties of the thermionic gun beam as input.

Fig. 8 GENESIS code results for the evolution of the e-beam microbunching fraction along the undulators using the measured properties of the thermionic gun beam as input.

Fig. 9 CTR spectrum (diamonds) and UR spectrum (dashes) obtained after undulator 5 using the microbunched PC gun beam. The narrowband CTR spectrum is at the SASE fundamental wavelength near 530 nm, but it is about 200 times weaker in intensity based on the ND filters employed. The alignment laser spectrum, (solid line) centered at 543.5 nm is also displayed in the plot for reference purposes.

Schematic of APS SASE FEL Experiment

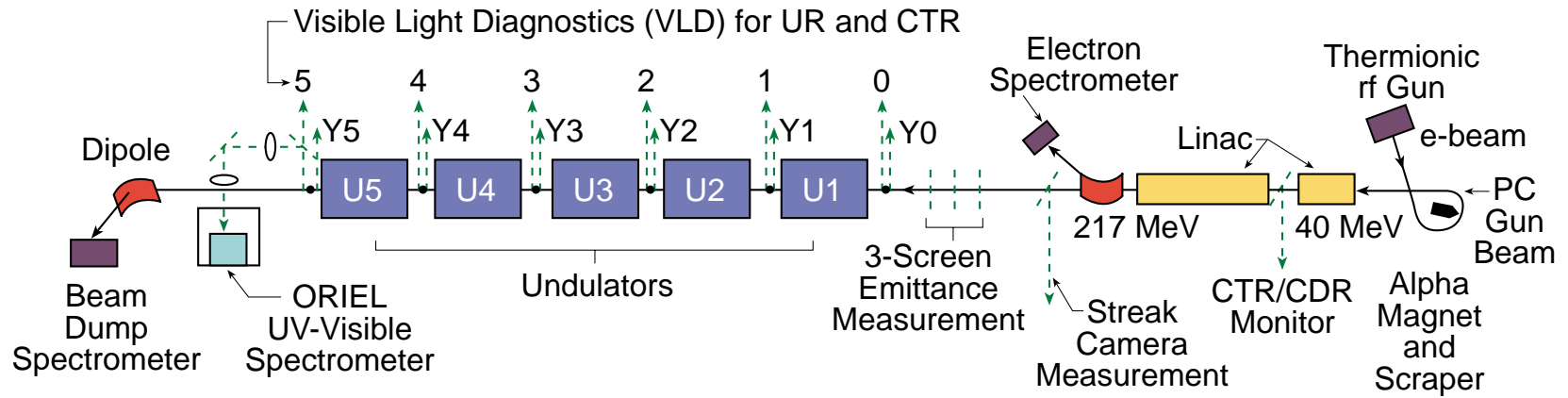


Figure 1

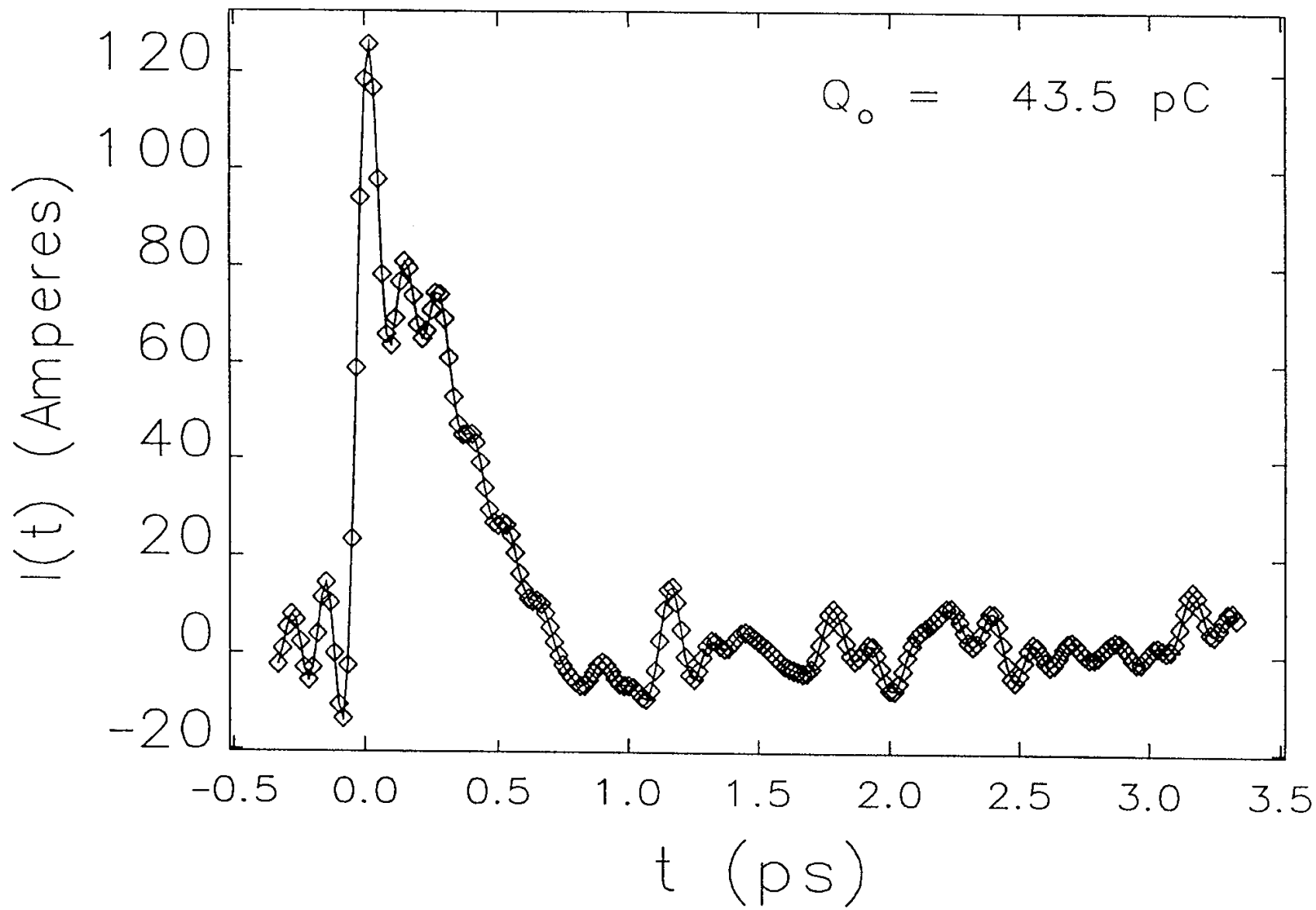


Figure 2

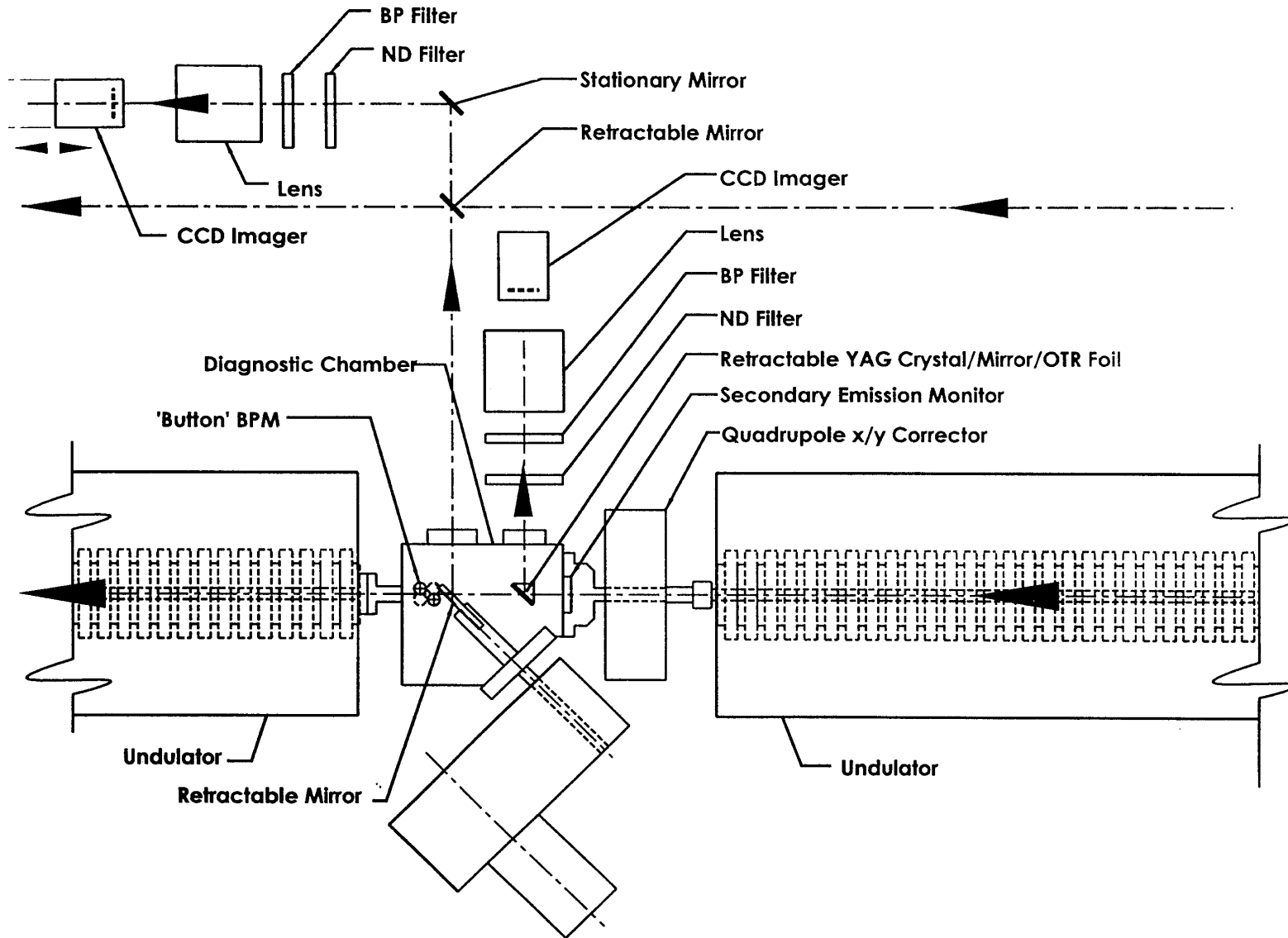


Figure 3

Examples of Angular Distribution Images along the Undulators (0, 3, 5) Show Enhancements (4-2-00)

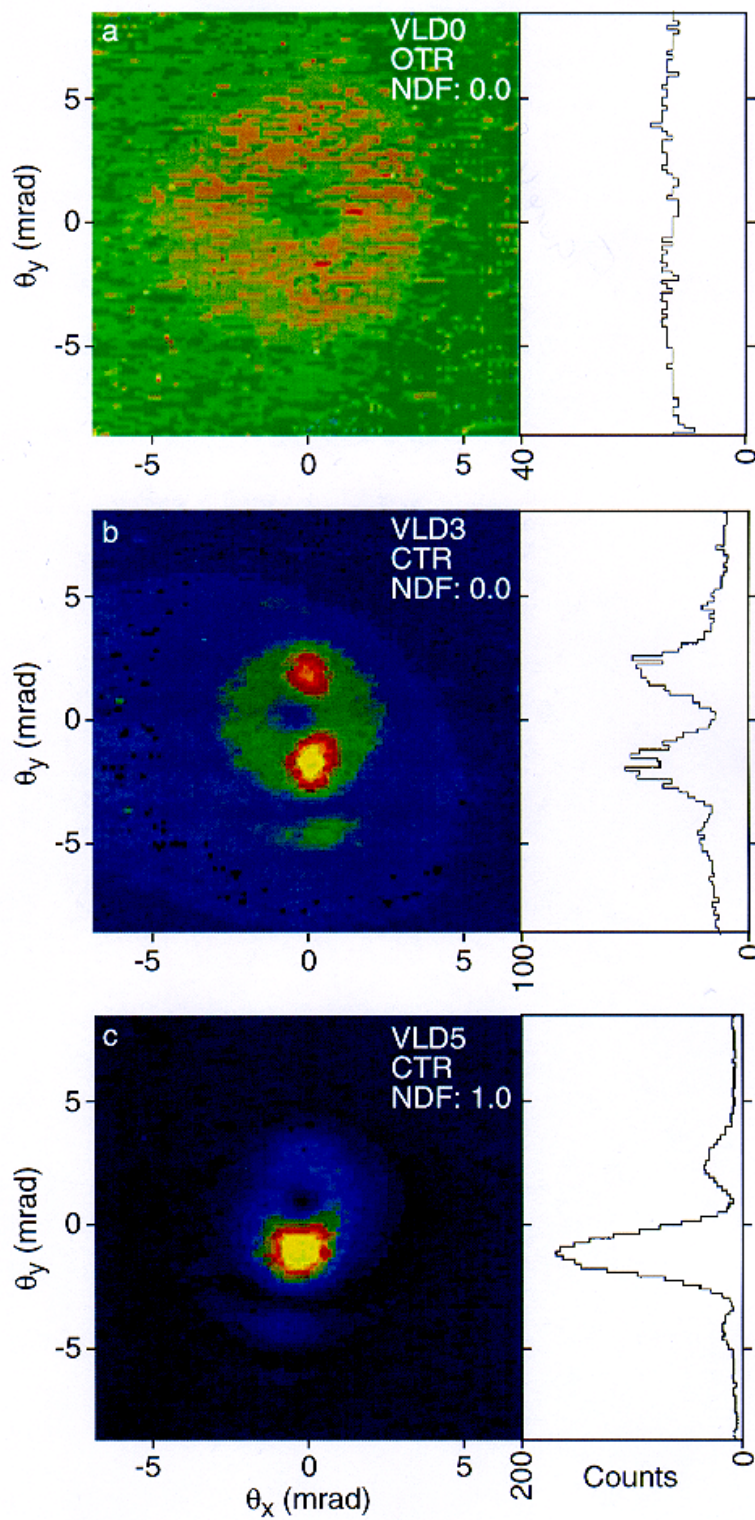


Figure 4

OTR Interferometer Calculation

(220 MeV, $S_{xy}=400$ urad, 500–580 nm, $D=6.3$ cm)

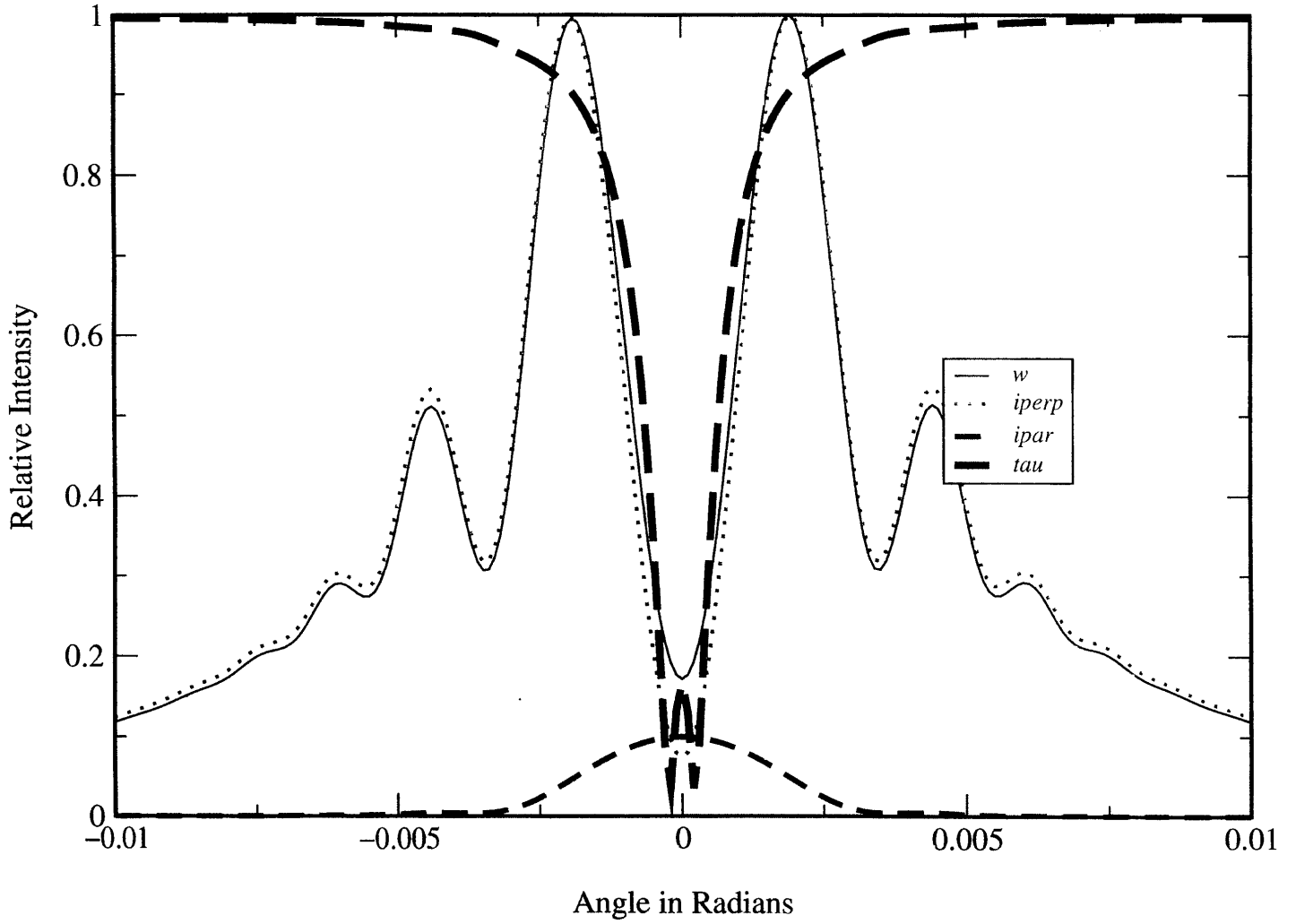


Figure 5

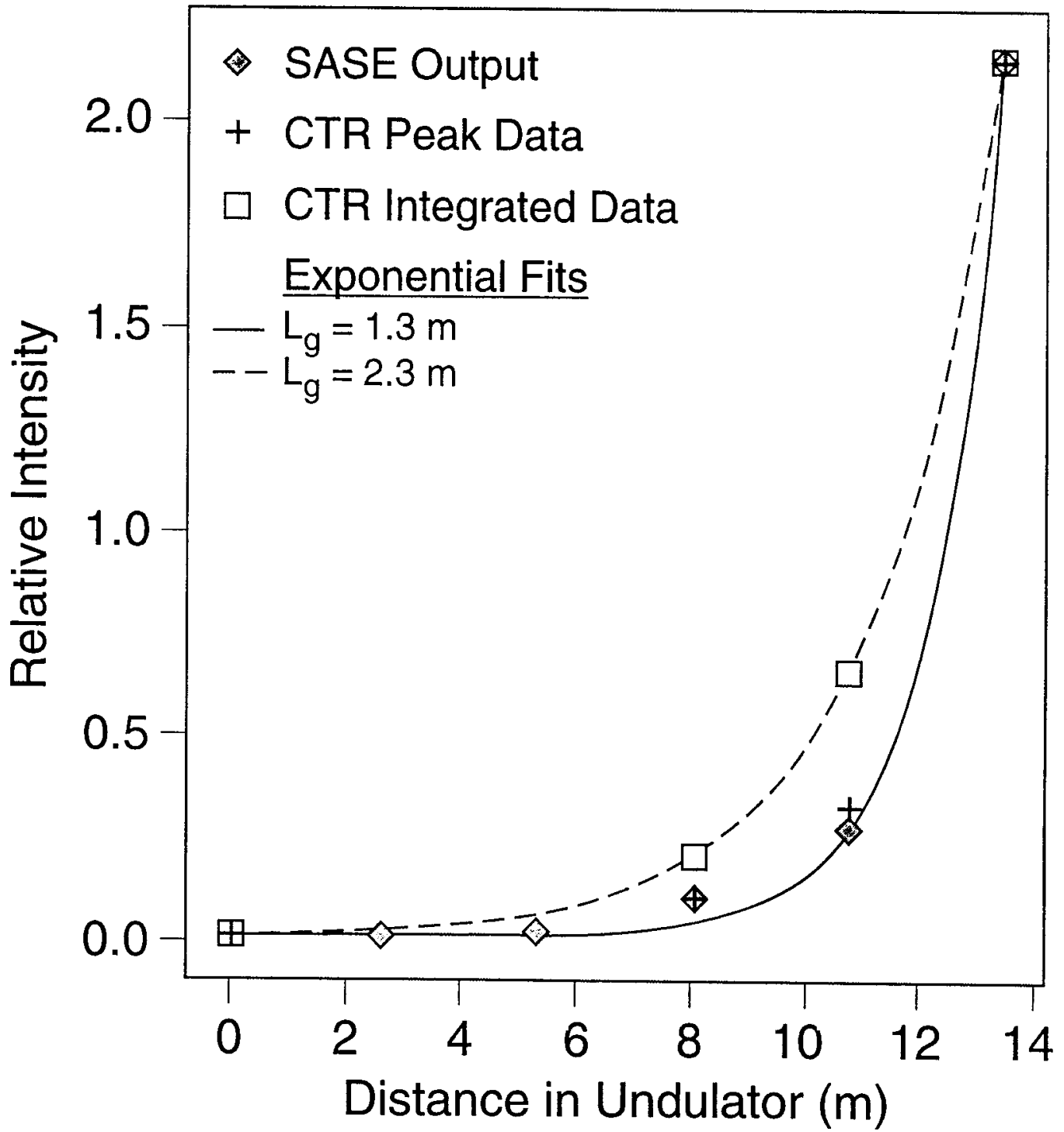
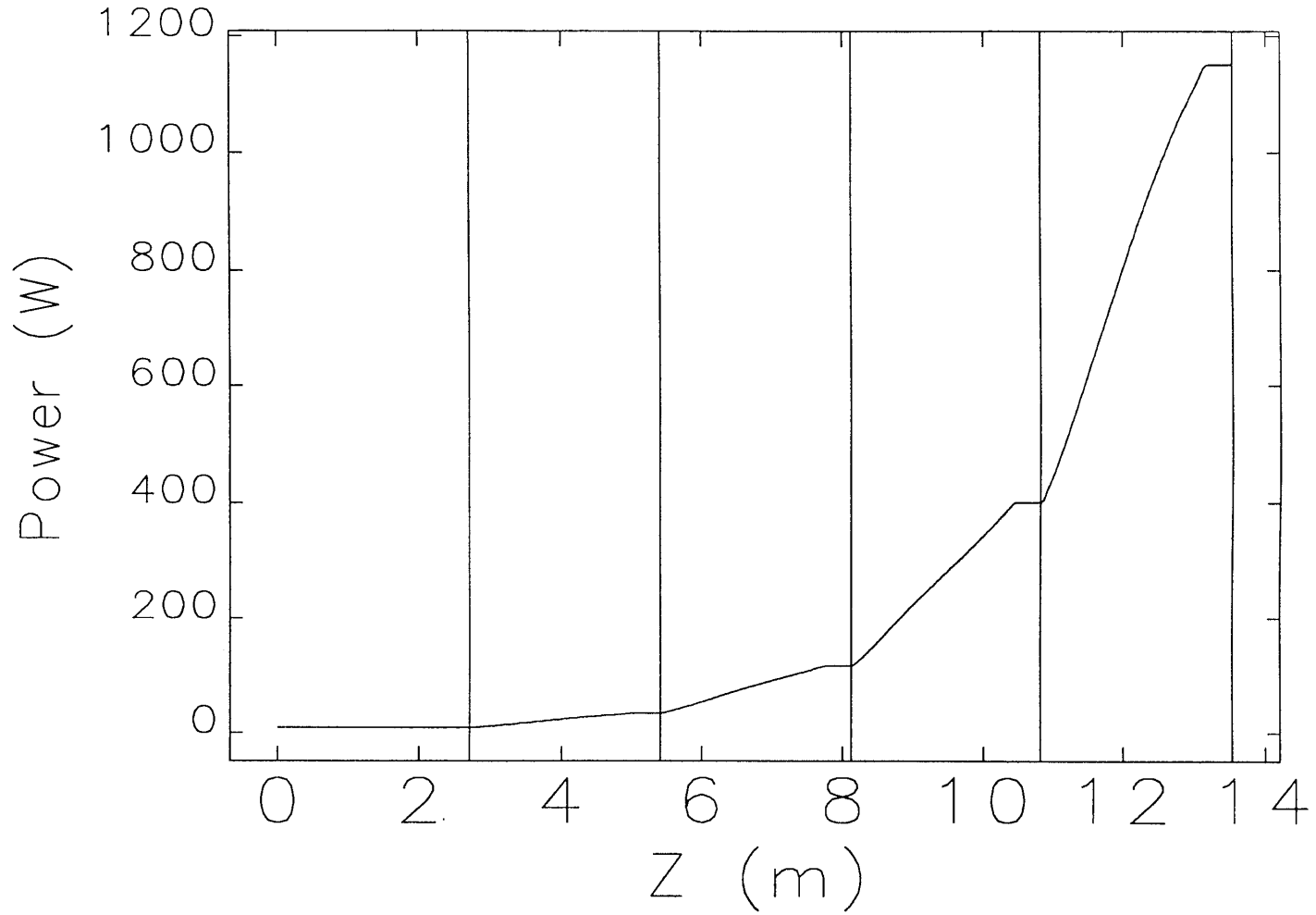
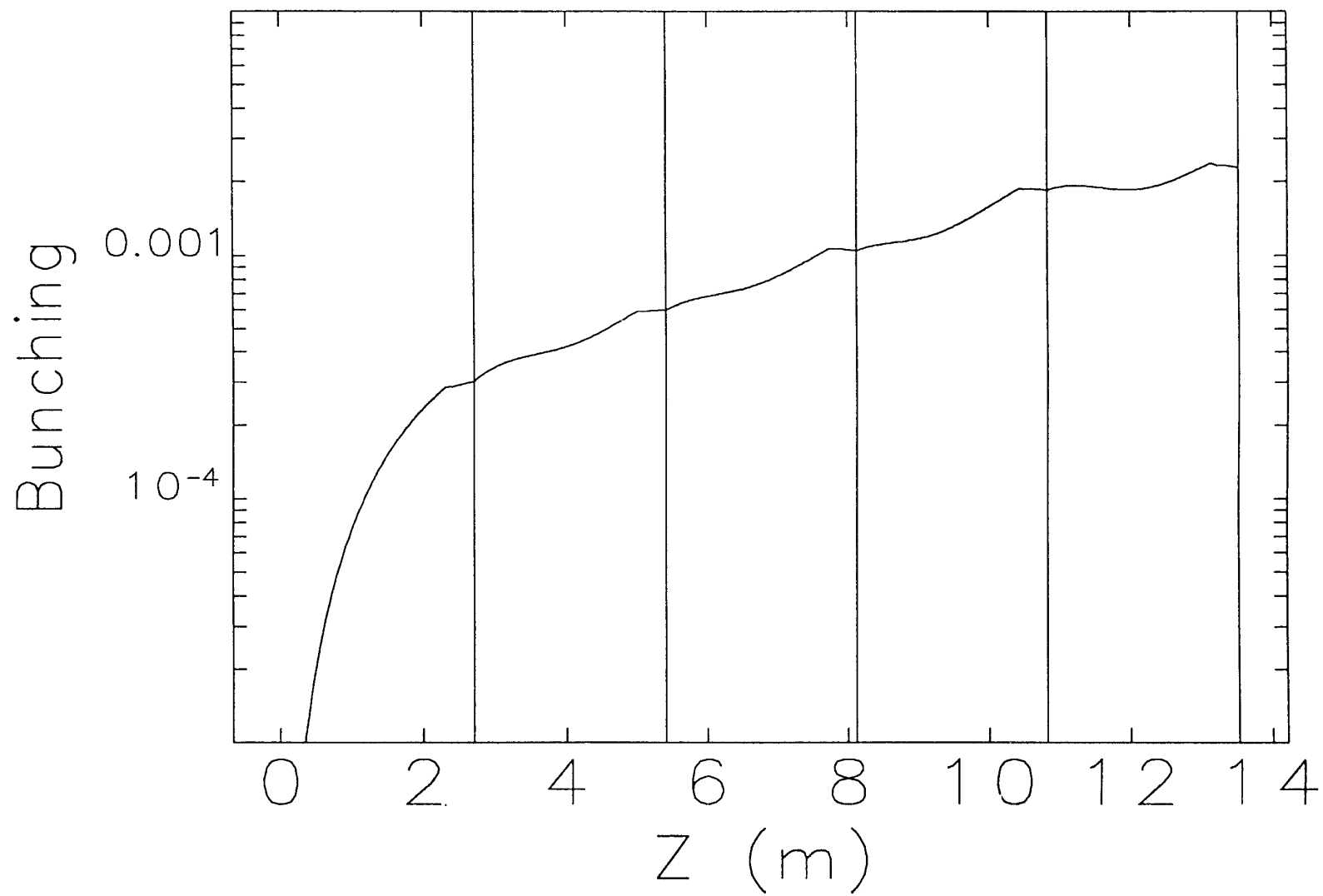


Figure 6



$E=21.7\text{MeV}, dE=0.1\%, I_p=100\text{A}, \epsilon_x=16.4\mu\text{m}, \epsilon_y=7.7\mu\text{m}, \lambda=532\text{nm}$

Figure 7



$E=21.7\text{MeV}, dE=0.1\%, I_p=100\text{A}, \epsilon_x=16.4\mu\text{m}, \epsilon_y=7.7\mu\text{m}, \lambda=532\text{nm}$

Figure 8

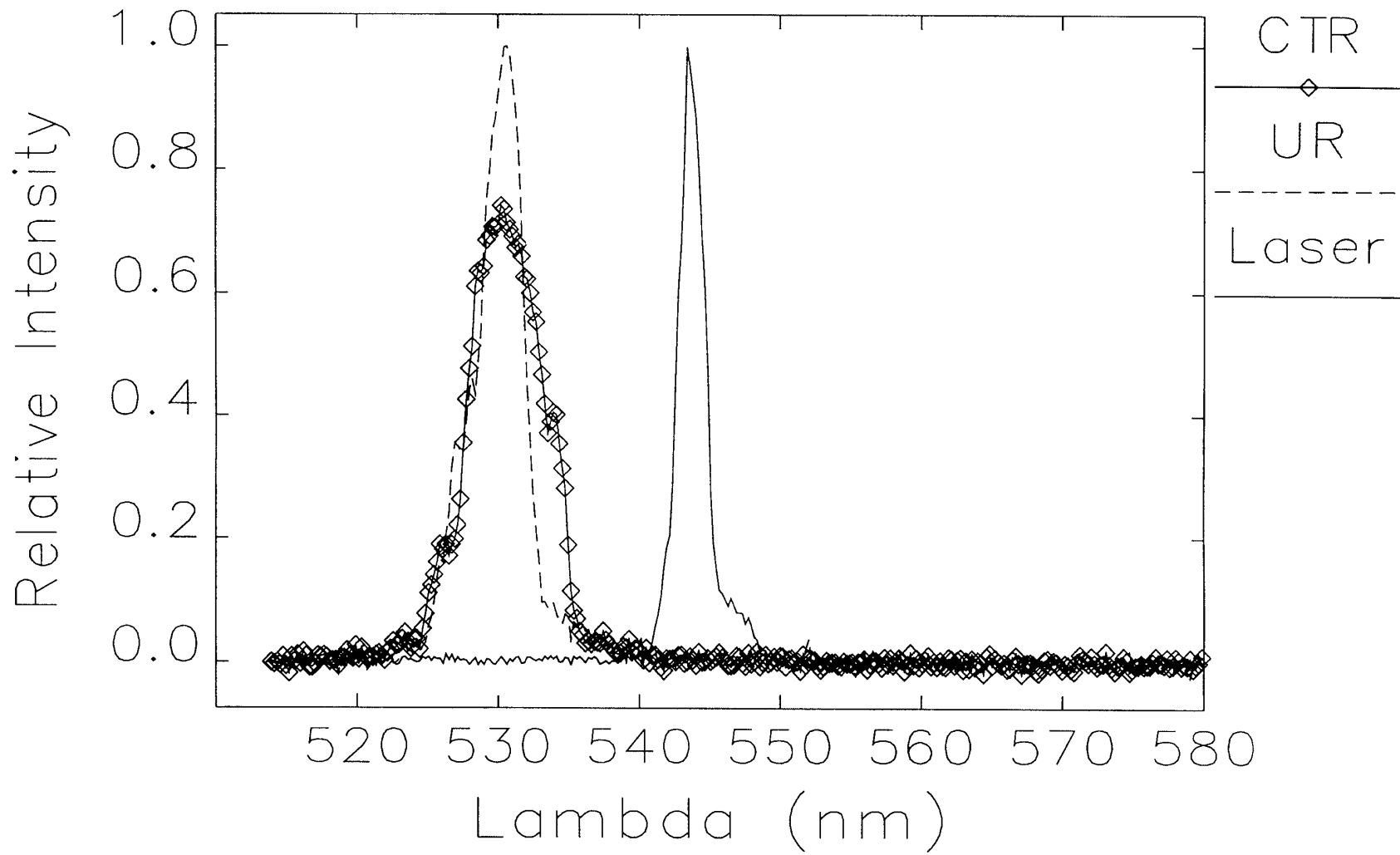


Figure 9